Supplement of Biogeosciences, 15, 3703–3716, 2018
https://doi.org/10.5194/bg-15-3703-2018-supplement

Biogeosciences Open Access EGU

Supplement of

Upside-down fluxes Down Under: CO_2 net sink in winter and net source in summer in a temperate evergreen broadleaf forest

Alexandre A. Renchon et al.

Correspondence to: Alexandre A. Renchon (a.renchon@gmail.com)

Contents:

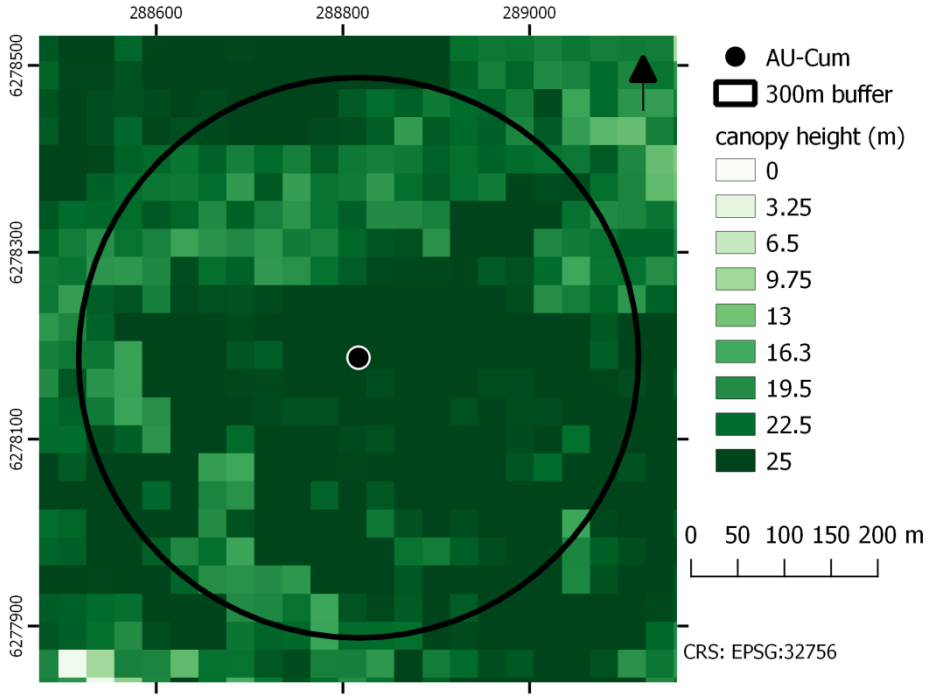

Figure S1 Canopy height model at AU-Cum site, generated at 30m spatial resolution using LiDAR data from 24.11.. The average canopy height was calculated to be 24.01m.

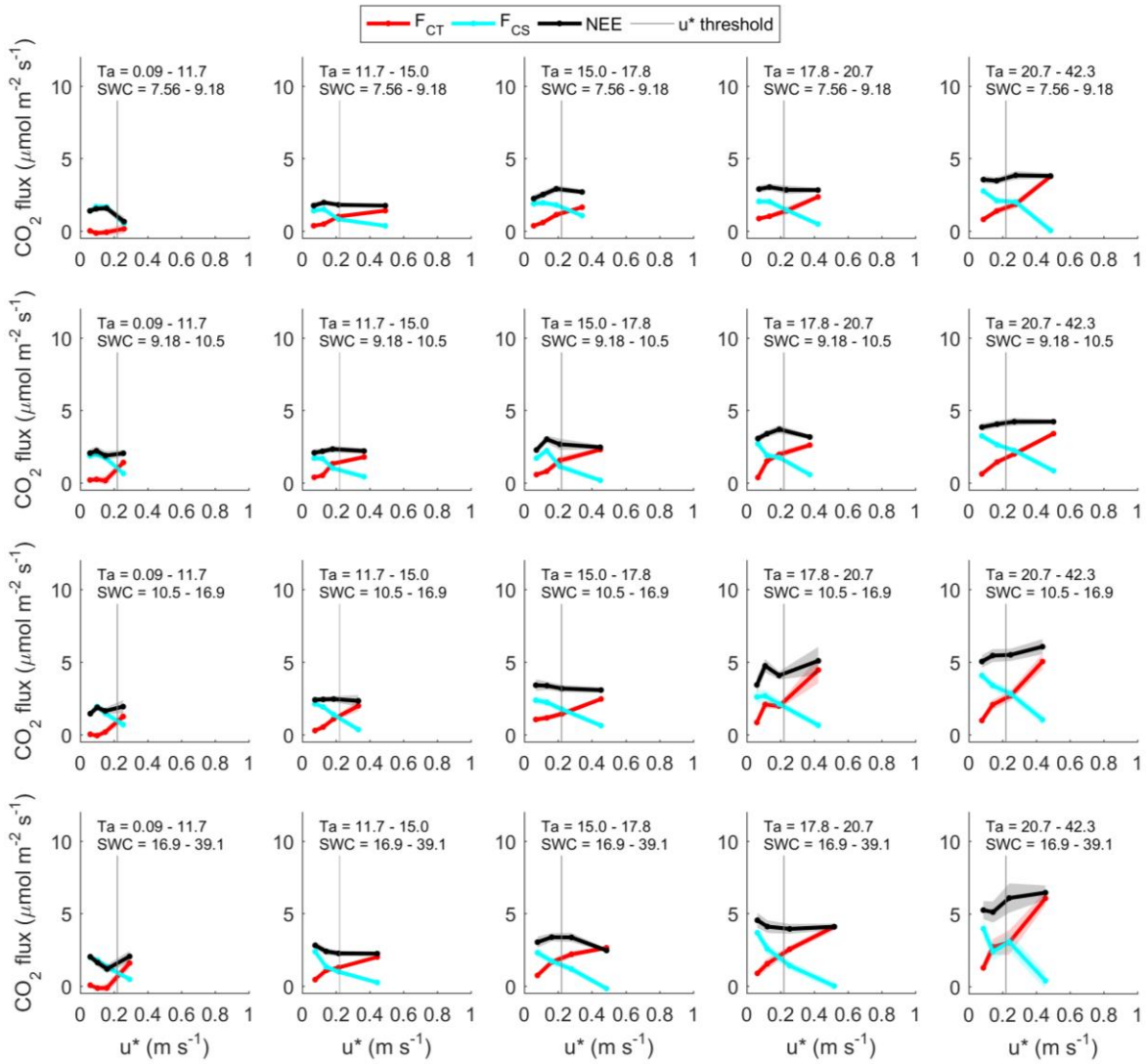

Figure S2 nighttime NEE (black), F_{CT} (red) and F_{CS} (cyan) vs. friction velocity (u*), per air temperature (T_a, left to right) and soil moisture quantiles (SWC, top to bottom). Actual values of T_a and SWC quantiles are shown in the figure. The vertical grey line show the u* threshold chosen to be conservative (no threshold detected using change point detection as NEE vs. u* was relatively flat for most T_a and SWC bins).

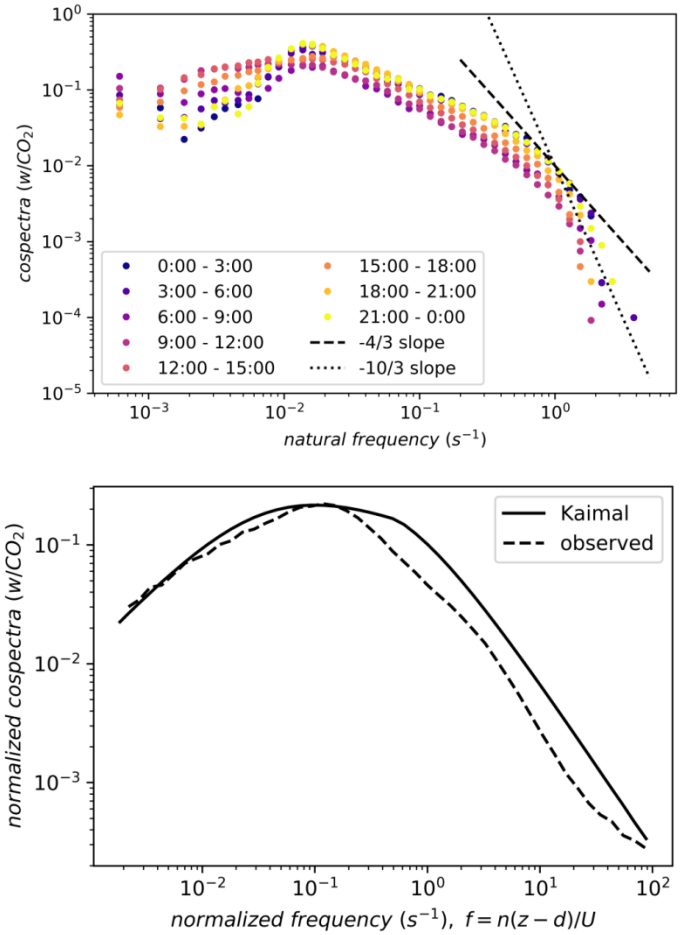

Figure S3 Top panel: 3-hourly binned w/CO_2 cospectra at AU-Cum. We observed the expected minor deviation from the 'ideal' -4/3 slope to a -10/3 slope in the high frequency domain due to the path length difference of the sonic anemometer and the IRGA (Burba 2013).
Bottom panel: comparison with the Kaimal model (Kaimal et al. 1972) did show the typical behaviour of tall towers. Observed CO_2 cospectras fall below the Kaimal model early as expected for tall towers, where some noise might be present in the signal.
These figures demonstrate that the reported fluxes are compliant with typical eddy covariance systems and hence are representative for the investigated ecosystem.

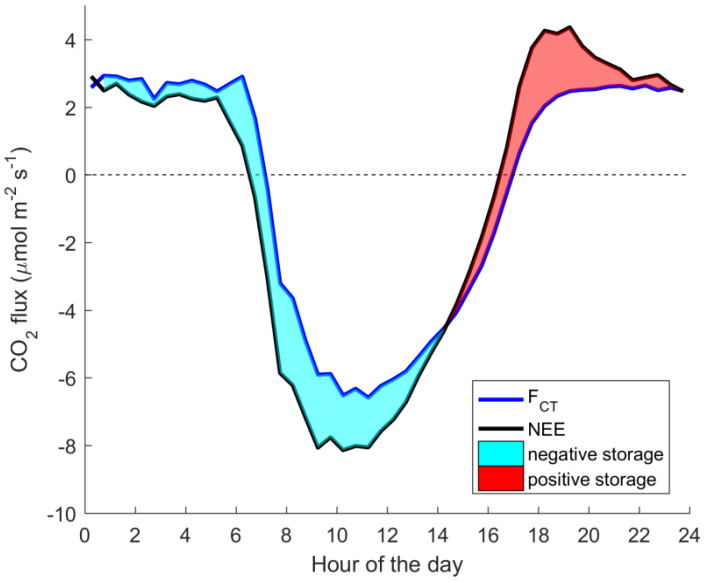

Figure S4 Diurnal course of all measured, quality checked and u* filtered net ecosystem exchange of CO_2 (NEE) and CO_2 vertical turbulent exchange (F_{CT}). The shading shows the change in storage term of the conservation of mass balance (F_{CS}, equation 1), cyan shading shows negative F_{CS} (CO_2 inside the control volume is decreasing) and red shading shows positive F_{CS} (CO_2 inside the control volume is increasing). Note that the storage flux is very impactful on flux rates during sunrise and sunset; not accounting for storage would drastically bias light response parameters.

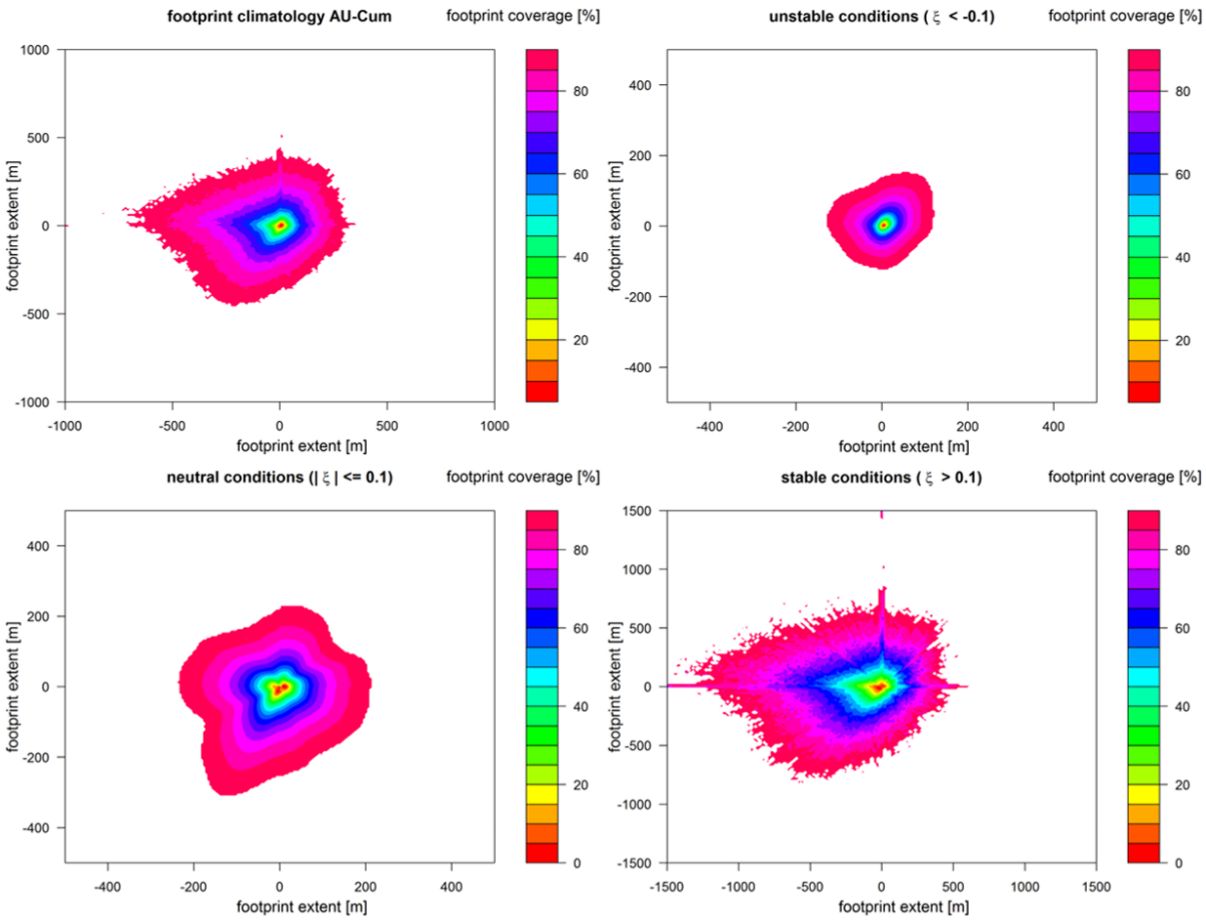

Figure S5 Footprint climatology at AU-Cum site, for all data, unstable, neutral and stable conditions. (Kormann and Meixner 2001) model was used, the figure was produced using FREddyPro package in R. Color show the footprint coverage in %, up to 90%. Note that the x-axis and y-axis scales (footprint extent, in m) change between subplots, as under stable conditions the footprint extends further from the tower.

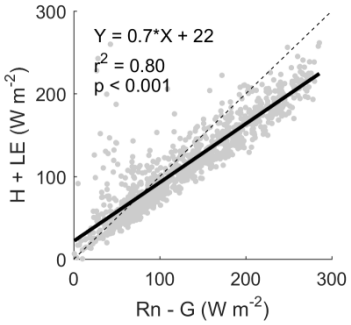

Figure S6 Energy balance closure (sensible + latent heat flux vs. net radiation - ground heat flux), daily data from 2014 through end of 2016. The black dotted line shows 1 to 1 line, the solid line shows linear regression ($y = 0.7x + 16$), $r^2 = 0.85$. Note that the closure deficit, about 30%, is comparable to what is obtained on most forested sites.

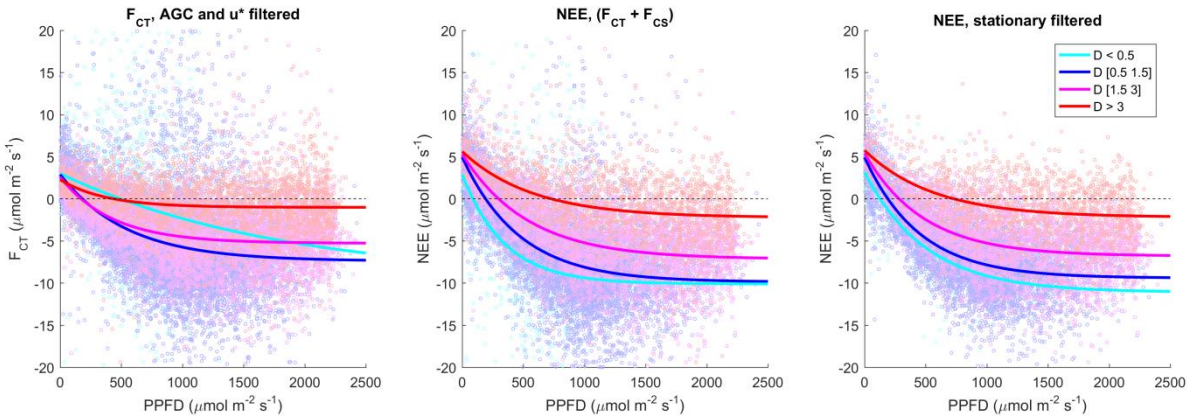

Figure S7 Light response of F_{CT}, NEE, and NEE after stationarity filter, colored by D. Line shows light response curve fits (Mitscherlich (1909); Eq. 5). Note that accounting for the change in storage flux (F_{CS}) is necessary for constraining light response parameters correctly; light response parameters using F_{CT} can lead to negative R_d or low D limiting photosynthesis, both are incoherent. Stationarity filter enhances the quality of NEE data. These two steps are particularly important under low D conditions (e.g., at sunrise, when PAR ~ 0, where data constrain both R_d and α).

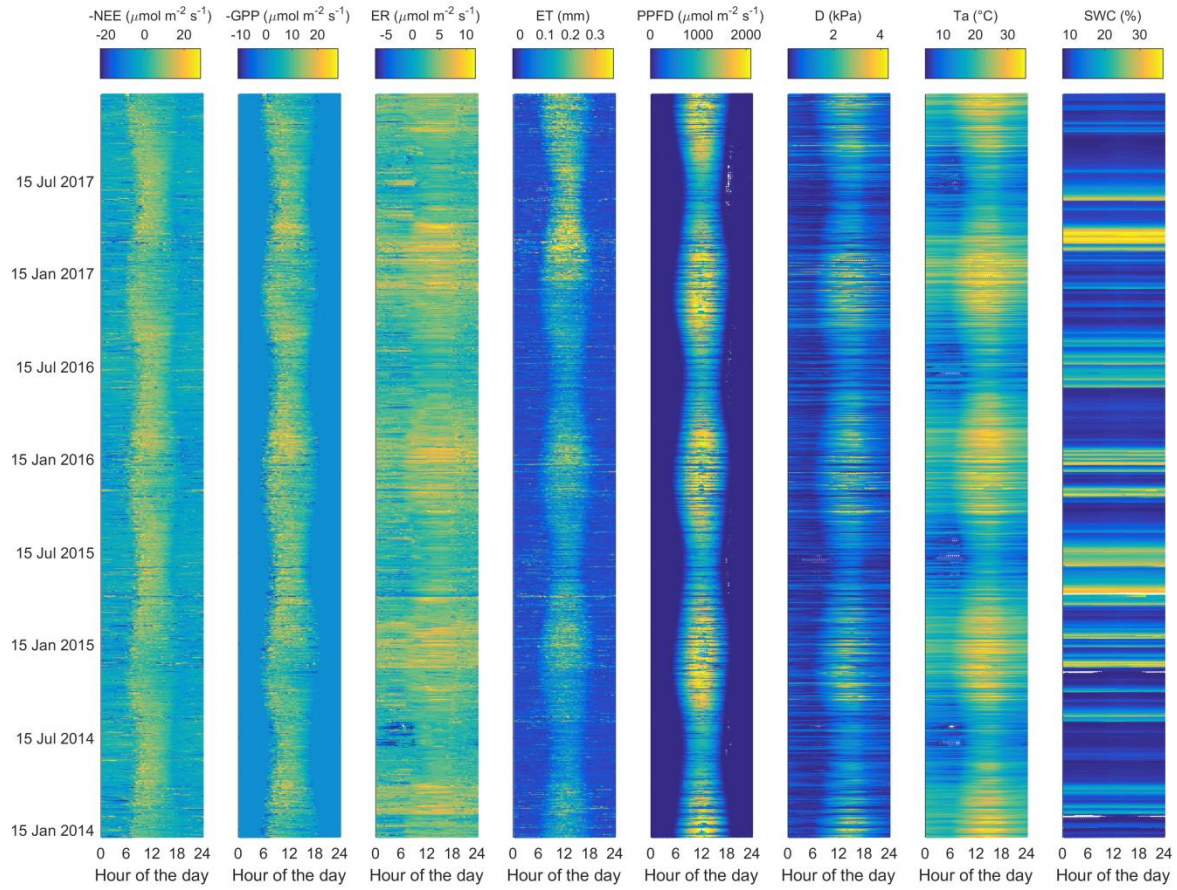

Figure S8 Time series (bottom: January 2014, top: January 2017) and diurnal course of fluxes and environmental drivers over the three years of the study. Note the reduced NEE and GPP in the afternoon during summer, despite estimated ER being higher (which would increase estimated GPP). Note the shorter day length and light intensity in winter. 98% of the data (> 0.01 quantile and < 0.99 quantile) is shown, in order to filter extreme value impacts on color-axis range.

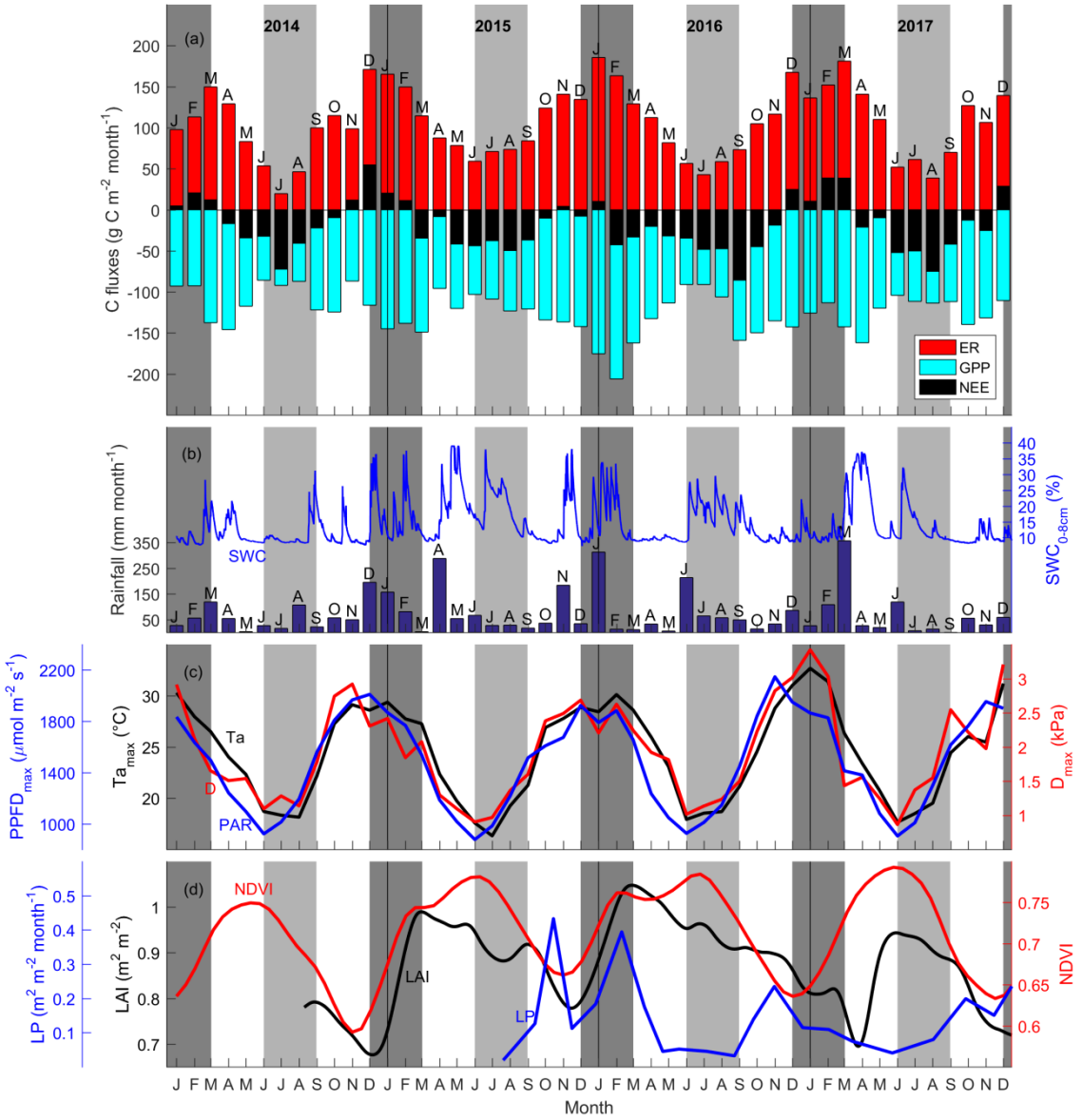

Figure S9a Similar to figure 1, but with NDVI instead of EVI in panel (d).
a) Time series of monthly carbon flux (net ecosystem exchange (NEE), ecosystem respiration (ER) and gross primary productivity (GPP), g C m^{-2} $month^{-1}$) (negative indicates ecosystem uptake); b) rainfall, mm $month^{-1}$; soil water content from 0 to 8 cm ($SWC_{0\text{-}8cm}$, %); c) average of daily maximum for each month photosynthetically active radiation ($PPFD_{max}$, µmol m^{-2} s^{-1}), air temperature (Ta_{max} , °C) and vapour pressure deficit (D_{max}, kPa)]. Canopy dynamics trends [normalised difference vegetation index (NDVI, unitless); d) leaf area index (LAI, m^2 m^{-2}) from November 2013 to April 2016 and litter production (LP, m^2 m^{-2} $month^{-1}$)]. Shaded areas shows summer (dark grey) and winter (light grey). Note Ta_{max} and $PPFD_{max}$ remained above 15 °C and 800 µmol m^{-2} s^{-1}.

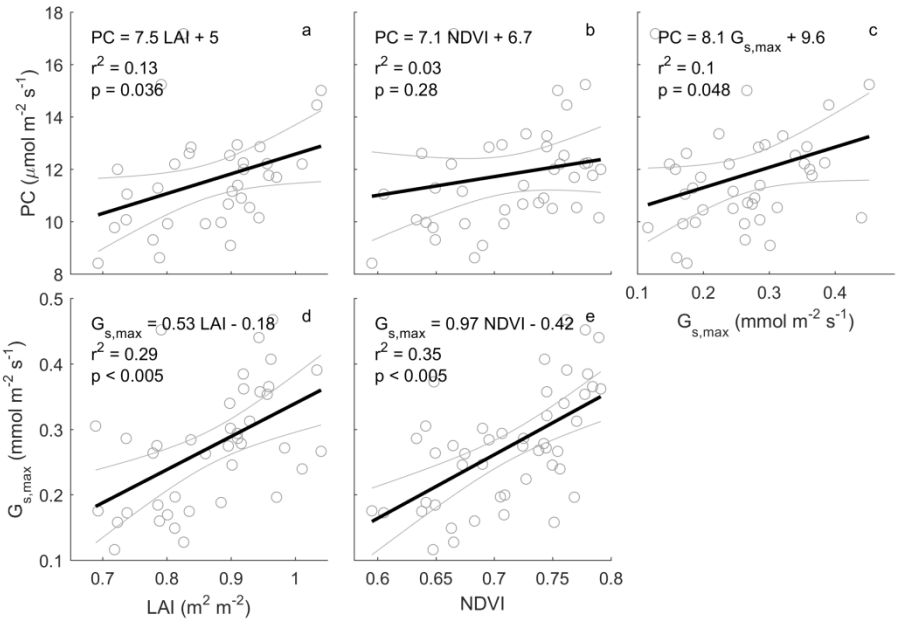

Figure S9b Similar to figure 6, but with NDVI instead of EVI.
Relationships between monthly photosynthetic capacity (PC, µmol m^{-2} s^{-1}), leaf area index (LAI, m^2 m^{-2}), 250 m^2 normalised difference vegetation index (NDVI), and maximum surface conductance ($G_{s,max}$). Monthly PC / $G_{s,max}$ are calculated as the median / 75% quantile of half-hourly GPP / G_s when PPFD [800-1200 µmol m^{-2} s^{-1}] and D [1-1.5 kPa]; rain events are filtered for $G_{s,max}$ estimation, to minimise evaporation contribution to evapotranspiration (see methods). Monthly LAI is calculated as mean of LAI smoothed by a spline. Thick black line shows a linear regression. For PC calculation, GPP data is only used when quality-checked NEE is available (GPP = NEE measured – ER estimated by a neural network, see method).

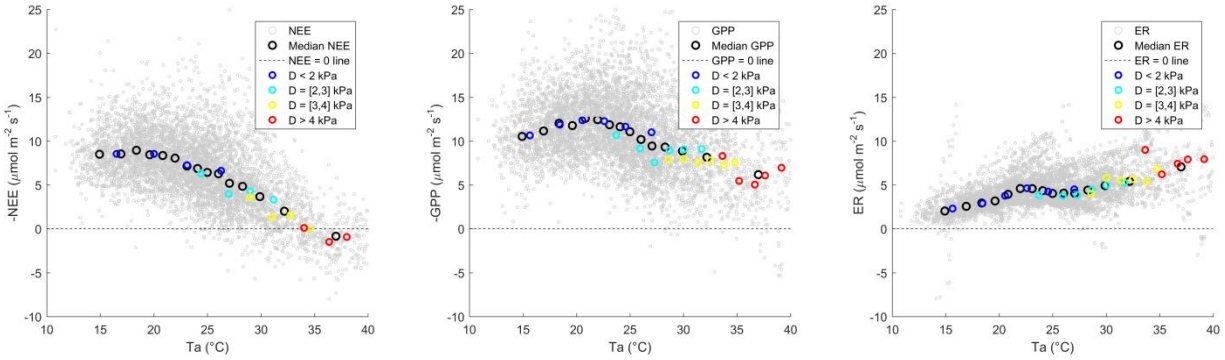

Figure S10 Light-saturated (photosynthetically active radiation (PAR) > 1000 µmol m^{-2} s^{-1}) C-fluxes: net ecosystem exchange (NEE), gross primary productivity (GPP) and ecosystem respiration (ER, from SOLO) versus air temperature. Grey dots are half-hourly measurements; black dots are C-flux for 15 T_a bins of equal sized n; colored dots are C-fluxes for 4 T_a bins within a D bin. Maximum light-saturated GPP rates occur around 22 °C, NEE becomes negative (net C source) at light saturation above 35 °C.

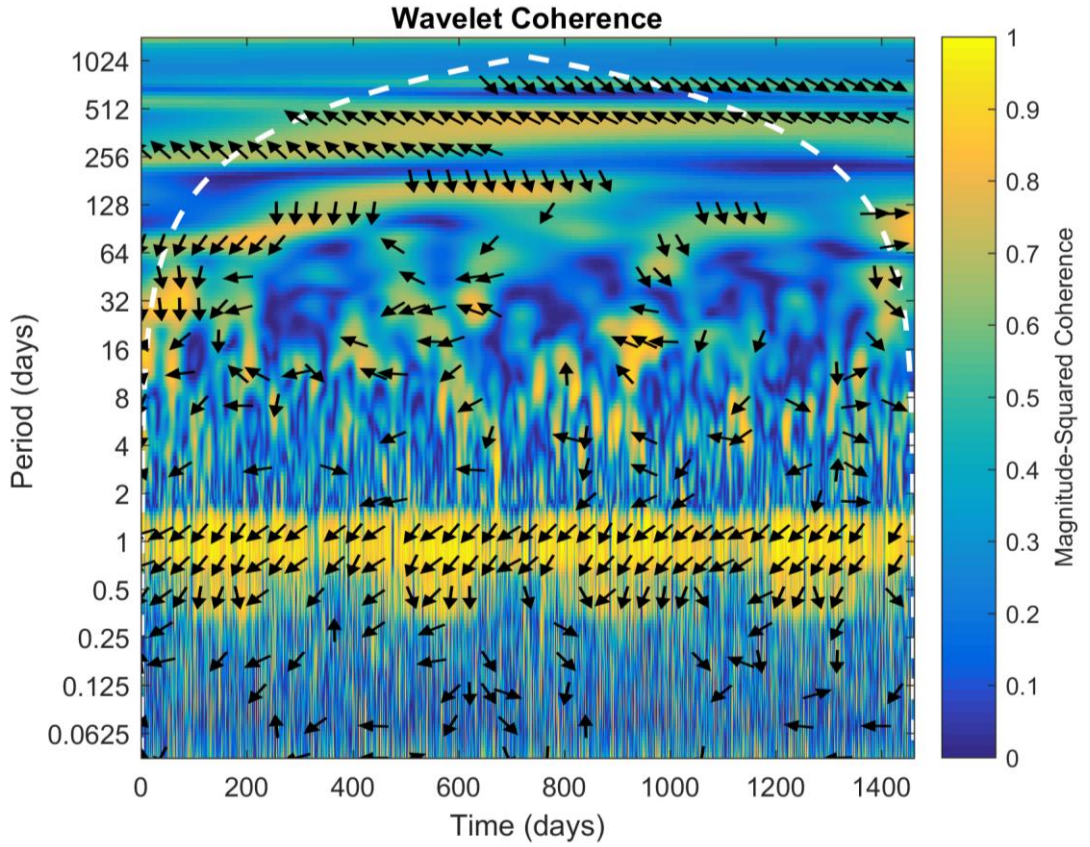

Figure S11 Wavelet coherence between D and GPP, for the four year study (2014 through 2017). The arrows represent the difference in phase between D and GPP for the specific time and period. Daily coherence is evident, which is expected as diurnal of D and GPP follow day/night cycle, the lag is due to GPP peaking around noon, while VPD peaks around 3pm. Similarly, annual coherence is high, as D and GPP are high in summer, low in winter. Some incursion of hot weather creates weekly coherences in summer, as GPP decreases when D increases.

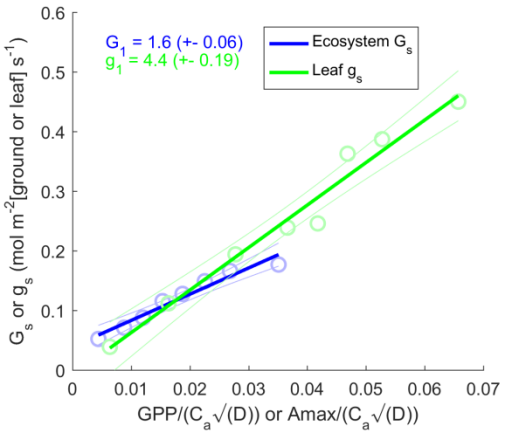

Figure S12 G_s or g_s vs. GPP or Amax/√D. g_1 and G_1 are estimated by solving equation (S1) or (S2) below. Eddy-covariance data filtered out periods after rain events (see surface conductance methods) in order to minimise contribution of soil evaporation to ET. G_s and g_s datasets are binned into 8 bins of equal size. Leaf-level data were measured at a site within 1.5km of the flux tower (Gimeno et al. 2016). Note the discrepancy between leaf level and ecosystem level g_1 and G_1, discussed in a recent study (Medlyn et al. 2017), where G_1 was found to be larger than g_1, which is opposite to our result.

$$G_s = G_0 + 1.6 \cdot \left(1 + \frac{G_1}{\sqrt{D}}\right)\frac{GPP_{max}}{400} \quad \text{(S1)}$$

$$g_s = g_0 + 1.6 \cdot \left(1 + \frac{g_1}{\sqrt{D}}\right)\frac{A_{max}}{400} \quad \text{(S2)}$$

References

Burba, G. 2013. Eddy covariance method for scientific, industrial, agricultural and regulatory applications: A field book on measuring ecosystem gas exchange and areal emission rates. LI-Cor Biosciences.

Gimeno, T. E., K. Y. Crous, J. Cooke, A. P. O'Grady, A. Ósvaldsson, B. E. Medlyn, and D. S. Ellsworth. 2016. Conserved stomatal behaviour under elevated CO2 and varying water availability in a mature woodland. Functional Ecology **30**:700-709.

Kaimal, J. C., J. Wyngaard, Y. Izumi, and O. Coté. 1972. Spectral characteristics of surface-layer turbulence. Quarterly Journal of the Royal Meteorological Society **98**:563-589.

Kormann, R., and F. X. Meixner. 2001. An analytical footprint model for non-neutral stratification. Boundary-Layer Meteorology **99**:207-224.

Medlyn, B. E., M. G. De Kauwe, Y. S. Lin, J. Knauer, R. A. Duursma, C. A. Williams, A. Arneth, R. Clement, P. Isaac, and J. M. Limousin. 2017. How do leaf and ecosystem measures of water-use efficiency compare? New Phytologist.